

12. The slope of the regression line of $\delta^{18}\text{O}$ versus the mixed-layer temperature is -0.20 for *G. ruber* and -0.19 for *G. sacculifer*, almost exactly the value predicted by Epstein *et al.* (6) in this temperature range, taking into account the quadratic term of the temperature equation. The correlation coefficients (r) are also at their highest values (Fig. 1). If the regression is made between $\delta^{18}\text{O}$ and the temperature (T) at 50 m, the correlation coefficients and the slopes of the regression lines decrease noticeably; the regression equations are $\delta^{18}\text{O}_{\text{ruber}} - \delta^{18}\text{O}_{\text{water}} = 0.97 - 0.16T$ ($r = .72$) and $\delta^{18}\text{O}_{\text{sacculifer}} - \delta^{18}\text{O}_{\text{water}} = 0.25 - 0.12T$ ($r = .61$). This poorer correlation is due to the fact that at those stations where the surficial mixed layer is shallower than 50 m, the temperature at 50 m is significantly lower than that of the mixed layer whereas the foraminiferal $\delta^{18}\text{O}$ value is similar to that of calcite secreted in warm waters. This result shows unambiguously that secretion occurs at (or close to) the temperature of the mixed layer and excludes the hypothesis that calcite is deposited at a constant depth (as shallow as 50 m), determined, for instance, by the extent of light penetration in the ocean.
13. In our measurements, the $\delta^{18}\text{O}$ values of foraminiferal shells from sediment samples are heavier than those of plankton samples by 0.78 per mil for *G. ruber* and by 0.92 per mil for *G. sacculifer*. A *t*-test performed on these differences gave *t* values of 8.79 for *G. ruber* and 10.16 for *G. sacculifer*. These high *t* values indicate that the mean differences are statistically different from zero, even at the confidence level of .995.
14. Mean values of $\delta^{18}\text{O}$ for foraminiferal shells from sediment samples are heavier than the calculated heaviest $\delta^{18}\text{O}$ values of shells secreted in surface water by 0.33 per mil for *G. ruber* and 0.60 per mil for *G. sacculifer*. A *t*-test performed on these differences gave *t* values of 4.77 for *G. ruber* and 11.73 for *G. sacculifer*. These high *t* values indicate that the mean $\delta^{18}\text{O}$ differences are statistically different from zero, even at the .995 confidence level.
15. W. H. Berger, *Mar. Geol.* 11, 325 (1971).
16. _____ and G. R. Heath, *J. Mar. Res.* 26, 135 (1968); T. H. Peng, W. S. Broecker, G. Kipputh, N. J. Shackleton, in *The Fate of Fossil Fuel CO₂ in the Oceans*, N. R. Andersen and A. Malahoff, Eds. (Plenum, New York, 1977), p. 355.
17. A. W. H. Bé, *Mar. Micropaleontol.* 5, 283 (1980).
18. The shells of plankton-tow specimens from the Barbados region have a mean isotopic composition of $\delta^{18}\text{O} = -2.54$ and $\delta^{13}\text{C} = +1.53$ prior to gametogenesis. The shells of living specimens from the same locality, grown in the laboratory and having undergone gametogenesis, had isotopic compositions of $\delta^{18}\text{O} = -2.33$ and $\delta^{13}\text{C} = -0.01$. Since we had no control over the isotopic composition of the culture water, we analyzed foraminifera grown in similar baths, which secreted several additional chambers before gametogenesis, producing a shell length increase from 51 to 332 percent. These shells had a mean isotopic composition of $\delta^{18}\text{O} = -0.95$ and $\delta^{13}\text{C} = -1.26$, an indication that the culture water was probably heavier by 1.6 per mil in $\delta^{18}\text{O}$ and lighter by 2.8 per mil in $\delta^{13}\text{C}$ than seawater. This experiment shows that the amount of gametogenic calcification is sufficient to account for a significant $\delta^{18}\text{O}$ enrichment of the foraminiferal carbonate shell.
19. A. W. H. Bé and O. R. Anderson, *Science* 192, 890 (1976).
20. We used the following formula

$$W = \frac{8}{3} \frac{v}{x} \left[-1 + \left(1 + \frac{1}{24} \frac{\rho_p \rho_E}{\rho_E} g \frac{x^3}{v^2} \right)^{1/2} \right]$$

where w is the speed of the particle; x is its mean diameter; ρ_p and ρ_E are the mass of a unit volume of the particle and seawater, respectively; g is the gravitational acceleration; and v is the seawater kinematic viscosity [J. C. Brun-Cottan, thesis, University of Paris (1976)]. Numerical values to be used are as follows: $v = 1.5 \times 10^{-2} \text{ cm}^2 \text{ sec}^{-1}$; $g = 981 \text{ cm sec}^{-2}$; $\rho_E = 1.03$; $\rho_p \approx 1.2$ (this low value reflects the occurrence of water which fills pores and the inside of the shell). The diameter x must be given in centimeters, and w has the dimensions centimeters per second.

21. A comparison of the size of *G. sacculifer* shells, measured by Bé (17), from plankton tows and from surface sediment off Barbados, shows that, on average, the shells are 18 μm larger in the sediment than in the plankton tows. This difference exactly matches an observed increase of 9 μm in the thickness of the last chambers of the sediment specimens compared to those of the plankton specimens. We devised a simple model

considering the pregametogenic adult shell as enclosing an immature shell (identical to those collected between 0 and 10 m) within larger final chambers (identical to those collected between 10 and 75 m). Assuming that the shell is constituted of spherical chambers, gametogenic calcification adds 22 percent to the pregametogenic shell and thus accounts for 18 percent of the weight of the postgametogenic shell, as found in the sediment.

22. Bé (17) compared the total weight of 50 pregametogenic specimens of *G. sacculifer* from a surface plankton tow collected off Barbados with the total weight of 50 postgametogenic specimens of *G. sacculifer* from the surface sediment from the same general location. The 50 specimens in each group were of the same size range and included the following shell lengths: 9 samples, 500 μm ; 13 samples, 520 μm ; 11 samples, 540 μm ; 7 samples, 560 μm ; 6 samples, 580 μm ; and 4 samples, 600 μm . The total weights of the pregametogenic and postgametogenic

groups were 1330 and 1700 μg , respectively. Thus, gametogenic calcification added 28 percent to the weight of the pregametogenic shells.

23. M. C. Bonneau, C. Vergnaud-Grazzini, W. H. Berger, *Oceanol. Acta* 3, 377 (1980).

24. W. H. Berger, J. S. Killingley, E. Vincent, *ibid.* 1, 203 (1978).

25. We thank J. C. Brun-Cottan for useful discussions, B. Le Coat and J. Antignac for help with the isotopic analyses, and M. Bé and S. Harrison for assistance in the micropaleontological analyses. Cruises *Osiris* II-MD 10 and *Osiris* III-MD 13 were sponsored by Les Terres Australes et Antarctiques Françaises. Laboratory studies were funded by the French Commissariat à l'Énergie Atomique, the Centre National de la Recherche Scientifique, and the U.S. National Science Foundation under grants OCE 78-25450 and OCE 76-02202. This report is Lamont-Doherty Geological Observatory contribution 3213.

17 March 1981

Radar Detection of Cloud-Seeding Effects

Abstract. *The effects on precipitation of artificially seeding clouds with Dry Ice have been monitored from cloud to ground with a radar that has a wavelength of 8.6 millimeters.*

The evaluation of the effects of artificial ice nucleants on clouds and precipitation is a difficult task that requires, in general, careful physical measurements and statistical evaluations (1). We describe here a powerful physical technique that utilizes an 8.6-mm-wavelength radar (2) with color display for detecting the effects of artificial seeding from cloud to ground (3).

To test the utility of the radar, we carried out a series of cloud-seeding trials in December 1979 and February 1980. The radar was located at Grayland, Washington, on the Pacific coast. In each trial an aircraft was used to seed layers of supercooled cloud with Dry Ice along tracks oriented perpendicular to

the wind direction and located at various distances upwind from the radar. The antenna of the radar was pointed vertically in order to detect the seeded tracks and unseeded portions of the cloud as they moved overhead. After seeding, the aircraft made a series of passes at different altitudes through the seeded and unseeded clouds in order to obtain detailed measurements of their microstructures (4).

During the course of the 2-month experiment, 108 tracks were seeded. We describe here the results obtained on 1 day.

On 20 February 1980 a broken, non-precipitating, altocumulus cloud deck was situated over Grayland. Cloud tops

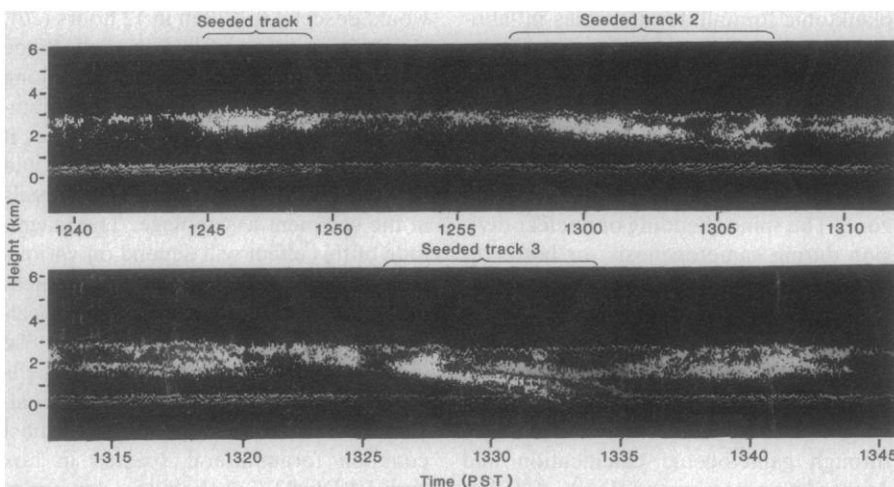


Fig. 1. Time-height display of radar echo pattern. The echo extending from ~ 0 to 0.5 km above ground is due to radar "ground clutter" and not to cloud. Clouds are located between ~ 5000 and 10,000 feet (~ 1.5 to 3 km). The gray areas represent the weakest radar echoes, black areas regions of intermediate radar echo strength, and white areas the strongest radar echoes. The third seeded track has precipitation falling from it that reached the ground at the radar site (see Fig. 3).

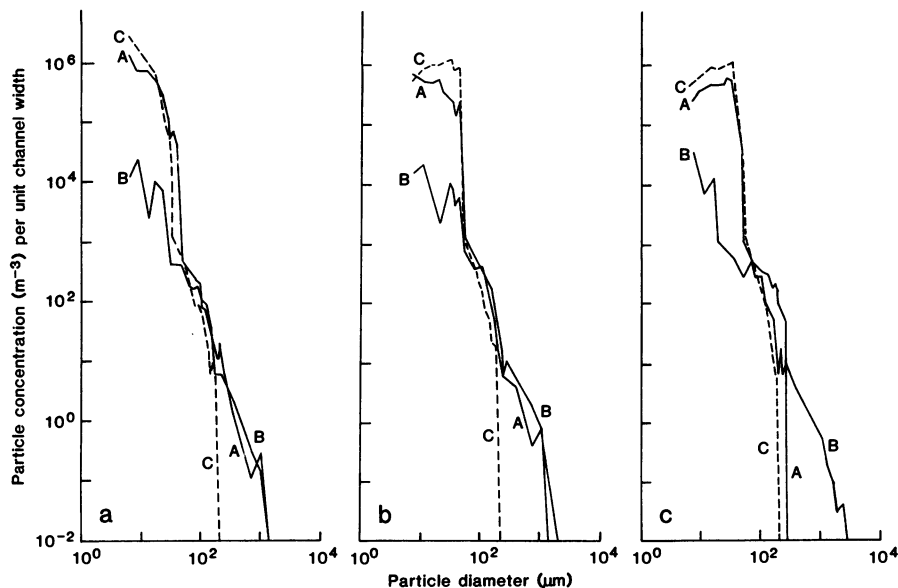


Fig. 2. Particle-size spectra measured during aircraft penetrations through the seeded (solid lines) and unseeded (dashed lines) clouds. (a) Track 1, pass A (2.3 km above MSL, -8.9°C , 33 minutes after seeding); track 1, pass B (2.0 km, -6.1°C , 39 minutes after seeding); pass C (2.4 km, -8.8°C) through an adjacent portion of nonseeded cloud. (b) Track 2, pass A (2.3 km above MSL, -9.3°C , 23 minutes after seeding); track 2, pass B (1.8 km, -5.8°C , 35.5 minutes after seeding); pass C (2.4 km, -9.9°C) through an adjacent portion of nonseeded cloud. (c) Track 3, pass A (2.4 km above MSL, -9.9°C , 7 minutes after seeding); track 3, pass B (1.6 km, -4.2°C , 41 minutes after seeding); pass C (2.5 km, -9.8°C) through an adjacent portion of nonseeded cloud.

were at an altitude of 2.5 km above mean sea level (MSL), where the temperature was -9.5°C . Winds were from 220° at 12 to 15 knots (6.2 to 7.7 m sec^{-1}). Prior to seeding, spectacular glories were observed from the aircraft flying above cloud top, revealing that the cloud contained fairly uniform water droplets (5). Seeding with Dry Ice was carried out at cloud top along several tracks located at various distances upwind of the radar. Measurements and observations on three of the seeded tracks will be described.

The first seeded track was situated 9 km upwind of the radar and was seeded at a rate of 0.05 kg of Dry Ice per

kilometer along a line 17 km long. This track passed over the radar between 1245 and 1248 PST about 21 minutes after it was seeded. As the seeded track passed over the radar, it produced an enhanced radar echo between altitudes of ~ 2 and 2.7 km above MSL (Fig. 1).

The first aircraft penetration of the seeded portion of the cloud was at an altitude of 2.3 km above MSL (-8.9°C) 33 minutes after seeding and 12 minutes after the seeded track had passed over the radar. The size spectrum of particles measured during this penetration is shown as curve A in Fig. 2a. The seeded cloud contained particles between 200 μm and 1 mm in size in measurable

concentrations, whereas the adjacent unseeded cloud (curve C) did not.

A second aircraft pass was made through the seeded cloud at an altitude of 2.0 km above MSL (-6.1°C) 39 minutes after seeding and 18 minutes after this cloud had passed over the radar (curve B in Fig. 2a). It shows concentrations of large particles similar to those of curve A, but the concentrations of smaller particles (< 50 μm) are much lower than those shown in either curve A or curve C. The progressive depletion of the smaller particles in the seeded cloud was no doubt due to their collection by the larger ice particles, since observations of the latter with instrumentation aboard the aircraft showed that they consisted of graupel-like particles and ice crystal aggregates. Precipitation particles from the seeded cloud, extending below cloud base but not reaching the ground, were observed visually from the aircraft after the cloud had passed over the radar.

The second track that was seeded was also located 9 km upwind of the radar; Dry Ice was again dispersed at a rate of 0.05 kg km^{-1} into cloud top, but the length of the seeded track was increased to 25 km. The seeded track passed over the radar 25 minutes after seeding (at 1257 to 1307 PST) and produced a more extensive radar echo than the first seeded track (Fig. 1). However, as was the case for the first track, no precipitation reached the ground at the radar site. The aircraft made four passes through the seeded cloud. The particle size spectra measured on two of these passes are shown as curves A and B in Fig. 2b. They reveal effects due to seeding very similar to those noted for the first seeded track: the appearance of large ice particles and subsequently depletion of the small particles. In this case, the measurements shown as curve A in Fig. 2b were obtained just 2 minutes before

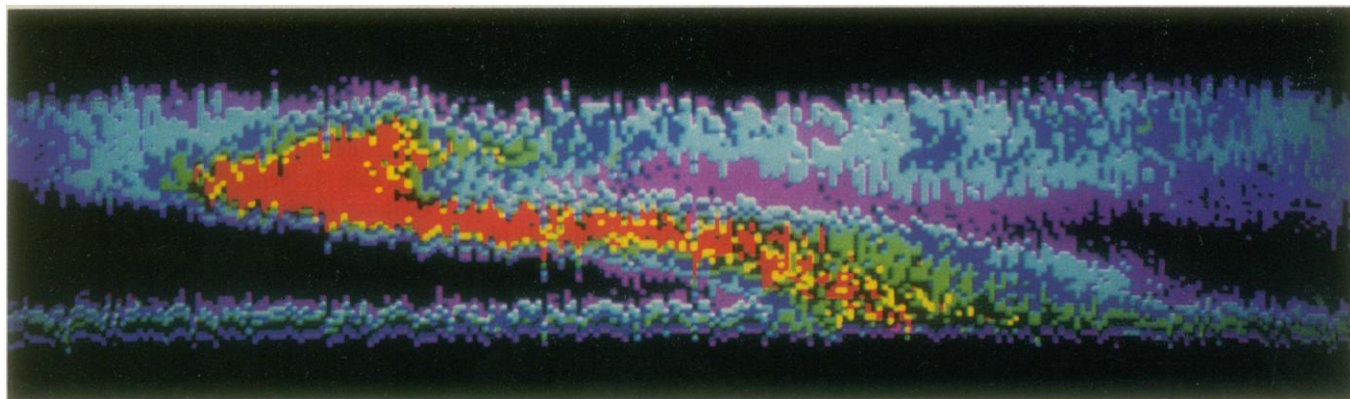


Fig. 3. A vertical cross section of the radar echo pattern of track 3 through a cloud. The natural cloud (purple and blue) is fairly uniform in structure and not precipitating. A portion of the cloud that was artificially seeded with Dry Ice produced a more intense radar echo (green, yellow, and red) and a trail of precipitation that reached the ground.

the seeded cloud passed over the radar.

The seeding of the two tracks described above produced significant changes in the structures of the clouds that enhanced their radar reflectivities. However, it appeared that the seeding was being carried out too close to the radar to allow sufficient time for the large particles produced by the seeding to reach the ground at the radar site. Consequently, the third seeded track was located 18 km upwind of the radar (twice the spacing used in the second track). In addition, the rate of Dry Ice seeding was doubled (to 0.1 kg km^{-1}).

The third seeded cloud passed over the radar between ~ 1326 and 1328 PST (~ 40 minutes after seeding). Precipitation trails from this cloud reached the ground between ~ 1331 and 1334 PST (Fig. 1). (An expanded view of the radar display of this seeded track is shown in Fig. 3, where various radar echo intensities are depicted in different colors.) The amount of precipitation that reached the ground at the radar site was quite small (observers on the ground reported a trace). The fact that the radar detected a strong signal all the way to the ground illustrates its sensitivity. The particle size spectra measured in this third seeded track are shown as curves A and B in Fig. 2c; curve C shows the measured spectrum in an adjacent cloud that was not seeded. The spectrum shown in curve B was measured at an altitude of 1.6 km above MSL (-4.2°C) just 1 minute after the seeded cloud passed over the radar. Aggregates of ice particles 2 mm in size in concentrations of ~ 30 per liter were measured on this pass.

Each one of the three seeded tracks passed over the radar within a few minutes of the times predicted by the scientist aboard the B-23 aircraft. These predictions were based on the location of the seeding with respect to the radar and the velocity of the winds.

These observations illustrate that a short-wavelength radar can provide a unique and powerful tool in evaluating the effects of cloud seeding. It permits continuous remote sensing of precipitable particles from cloud to ground, a capability that thus far has not been used in cloud-seeding research.

PETER V. HOBBS
JAMIE H. LYONS
JOHN D. LOCATELLI
KUMUD R. BISWAS
LAWRENCE F. RADKE
RICHARD R. WEISS, SR.
ARTHUR L. RANGNO

Atmospheric Sciences Department,
University of Washington,
Seattle 98195

References and Notes

1. R. R. Braham, Jr., and commentators, *J. Am. Stat. Assoc.* **74**, 57 (1979).
2. Our 8.6-mm-wavelength radar is an adaptation based on the use of modern technology of the AN/TPQ-11 radar developed by the Air Force [W. H. Paulsen, P. J. Petrocchi, G. McLean, *Operational Utilization of the AN/TPQ-11 Cloud-Detection Radar* (Instrumentation Papers, No. 166, Air Force Cambridge Research Laboratories, L. G. Hanscom Field, Bedford, Mass., 1970)].
3. There have been a few reports describing the use of radars with wavelengths of several centimeters for detecting precipitation produced by artificial seeding. For example, D. Atlas [*Bull. Am. Meteorol. Soc.* **46**, 696 (1965)] mentioned some demonstrations of this type in the Soviet Union. P. V. Hobbs [*J. Appl. Meteorol.* **14**, 805 (1975)] described the use of a 3.2-cm Doppler radar for detecting changes in particle fallspeeds produced by seeding. However, to our knowl-
- edge, the radar measurements reported here are unique in documenting the effects of cloud seeding from cloud to ground.
4. The University of Washington's B-23 research aircraft was used in these experiments. The extensive instrumentation aboard this aircraft for measuring the properties of clouds and precipitation has been described by P. V. Hobbs, T. J. Matejka, P. H. Herzegh, J. D. Locatelli, and R. A. Houze, Jr. [*J. Atmos. Sci.* **37**, 568 (1980)].
5. R. A. R. Tricker, *Introduction to Meteorological Optics* (American Elsevier, New York, 1970), pp. 191-209.
6. Supported by the Atmospheric Research Section of the National Science Foundation (ATM8013125), the Pacific Northwest Regional Commission (grant 10990022), and the Bonneville Power Administration (contract DE-AC79-80BP 18278). Contribution No. 572 of the Atmospheric Sciences Department, University of Washington.

23 January 1981; revised 27 March 1981

Sodium Pump in Skeletal Muscle: Central Nervous System-Induced Suppression by α -Adrenoreceptors

Abstract. *The central nervous system regulates active sodium and potassium transport in rat skeletal muscle during hypokalemia. This regulation is achieved by the apparent release of catecholamines onto muscle following nerve activity. This effect can be prevented by treatment with agents that block the α -adrenoreceptor.*

Potassium-deficient diets cause a decrease in K^+ concentration in blood plasma and skeletal muscles but not in cerebrospinal fluid or brain tissue. During the first 4 to 5 weeks of potassium deficiency, decreases in the rat muscle K^+ are not compensated by equivalent increases in muscle Na^+ . However, during further hypokalemia, the ratio of the number of Na ions entering the muscle to that of K ions coming out approaches one (1). The plasma K^+ concentration in hypokalemic rats decreases from a normal level of about 4.6 mM to about 1.6 mM, a value that is sufficiently high to maintain activity of the Na-K pump in muscle. Furthermore, when muscles from hypokalemic rats are excised and placed in a Krebs solution at 37°C , the intracellular Na^+ concentration, $[\text{Na}]_i$, is promptly reduced, whereas the intracellular K^+ , $[\text{K}]_i$, is increased even when the external K^+ concentration is as low as 1 mM (2). Therefore, in hypokalemic rats the high $[\text{Na}]_i$ and low $[\text{K}]_i$ of muscles in situ cannot be attributed to pump inhibition by plasma hypokalemia; there must be an additional mechanism by which activity of the Na-K pump in muscle of hypokalemic rats is suppressed in vivo.

We report here that sectioning of a peripheral nerve, decerebration, or spinal transection can remove suppression of the active Na-K transport in rat soleus muscle during hypokalemia and that the neurally mediated inhibition of the muscle Na-K pump is also abolished by α -adrenoreceptor blocking agents.

The experiments were performed on

soleus muscles of male Wistar rats that had been given free access to a potassium-deficient diet and deionized water for 5 to 7 weeks. Chemical analysis of Na^+ and K^+ contents in muscles and plasma samples were carried out with a flame spectrophotometer. The $[\text{Na}]_i$ and $[\text{K}]_i$ of tissues were calculated from the tissue cation contents, plasma cation contents, extracellular space, and the ratio of dry weight to wet weight according to the conventional method described by Desmedt (3).

The most striking finding was a dramatic reversal of the effects of hypokalemia on muscle $[\text{Na}]_i$ and $[\text{K}]_i$ by the sectioning of the tibial nerve branch or the sciatic nerve (Fig. 1 and Table 1) (4). After denervation, the soleus muscles promptly restored their $[\text{Na}]_i$ and $[\text{K}]_i$ to values close to those of "fresh" soleus muscles of normal rats (5). The half-recovery time of these internal cations was about 20 minutes. The recovery values leveled off within a few hours after denervation and the recovered $[\text{Na}]_i$ and $[\text{K}]_i$ remained unchanged for several days. The results under different experimental conditions are summarized in Table 1. When ouabain, a specific inhibitor of the Na-K pump, was administered prior to denervation, there was no recovery of the effects of hypokalemia on $[\text{Na}]_i$ or $[\text{K}]_i$ after denervation (see Table 1). Thus, the ouabain-sensitive Na-K pump must be involved in the denervation-induced recovery of the sodium and potassium contents of the muscle of hypokalemic rats.

Further characterization of the neural